International Journal of Applied Engineering Research ISSN 0973-4562 Volume 10, Number 21 (2015) pp 42099-42102

GIS application for NDVI calculation using Landsat 8 OLI images

P. D'Allestro,

PhD Student, Department of Sciences and Technologies, University of Naples "Parthenope", Naples Italy, pamela.dallestro@uniparthenope.it

C. Parente,

Associate Professor, Department of Sciences and Technologies, University of Naples "Parthenope", Naples Italy, claudio.parente@uniparthenope.it

Abstract
NDVI (Normalized Difference Vegetation Index) is easily calculated using the reflectance images of the scene in red and infrared bands. It permits to detect the vegetation areas (forests, grasses, groves, …) as well as to distinguish waters (oceans, seas, lakes, rivers, …) and soils (rocks, buildings, roads, …). Images supplied by Landsat 8 OLI (Operational Land Imager) sensor in the bands 4 and 5 can be used for NDVI calculation, deriving by digital numbers the solar radiation incident on the satellite sensor (Top Of Atmosphere, TOA). This paper is aimed to demonstrate that this transformation can be easily operated in GIS that also permits to implement NDVI formula. Landsat 8 OLI red and near-infrared images of Campania areas around the Gulf of Naples were considered: NDVI was calculated using TOA transformation of the original data. Classification of these data was applied to distinguish three homogeneous classes such as bare soil, water (sea and lakes) and vegetation.

Keywords-NDVI; TOA; Landsat 8 OLI images; reflectance; vegetation map

Introduction

Solar radiation in the visible spectral region (VIS) is used by live green plants as a source of energy in the process of photosynthesis, while that in the near-infrared (NIR) spectral region is reflected or transmitted by leaves. For consequence areas covered by vegetation are relatively dark in the VIS images and relatively bright in the NIR ones [1], [2].
Normalized Difference Vegetation Index (NDVI) is a good measure of the physiological activity of plants and also permits to distinguish waters as well as bare soils. Its values range from-1 to 1: because of their relatively high near-infrared reflectance and low red reflectance, vegetated areas generally return NDVI high values; rock and bare soil areas have similar reflectances in the two bands and produce values near zero; water, clouds, and snow have larger reflectance in Red than in NIR, so these features present negative values [3].
For NDVI calculation two images of the same scene, simultaneously acquired, one concerning the reflectance in Red, the other in NIR are necessary. This opportunity has been given by Landsat program since early '70 years. In fact Bands MultiSpectral Scanner (MSS) onboard of Landsat 1, Landsat 2 and Landsat 3 used a band-naming convention of MSS-4, MSS-5, MSS-6, and MSS-7 for the Blue, Green, Red, and NIR bands, respectively [4]; particularly MSS-6 and MSS-7 were used for NDVI first applications [5]. Red and NIR bands were included also in MSS sensors on board of Landsat 4 and Landsat 5 as well as in the other sensors on board of the satellites of the subsequent missions, including the latest Landsat 8. Landsat program has acquired a very important role to map land and vegetation cover change [6]. Relevant performances are confirmed by Landsat 8 OLI (Operational Land Imager): the new sensor has better capability in land surface process monitoring, such as land cover mapping, spatiotemporal dynamics of vegetation growth, and drought assessment as confirmed by greater Landsat 8 OLI NDVI higher spatial variability and contrast between vegetated areas and water areas [7].
Software for remote sensing applications already provides commands for NDVI calculation, but this formula can be easily implemented using GIS (Geographic Information System) tools for raster algebra that also permit to implement other calculations for performing results [8], [9].
This paper is focused on the possibility to process Landsat 8 OLI Infrared and Red images using ArcGIS, one of the most used GIS software by ESRI [10], to calculate NDVI. Applications were conducted on clipped imagery concerning the Province of Naples (Italy): original DNs (Digital Numbers) were transformed in TOA (Top of Atmosphere) Reflectance, the solar radiation incident on the satellite sensor, using formula by U. S. Geological Survey (USGS) [11]. Classification of NDVI map so to obtain three homogenous classes (waters, bare soils, vegetated areas) was carried out: Maximum Likelihood algorithm was used to define thresholds and results were tested considering confusion matrix indices (User Accuracy, Producer Accuracy and Overall Accuracy).

Data and methods

Landsat 8 OLI images

The multispectral and digital Landsat 8 images are more recent in the Landsat program, a joint effort of the U. S. Geological Survey (USGS) and the National Aeronautics and Space Administration (NASA) to monitor Earth from space [12].
On the 11 February 2013, the Landsat 8 satellite (fig. 1) was launched from Space Launch Complex 3E; its orbit is polar sun-synchronous at 705 kilometers (438 miles) altitude. Every 99 minutes this satellite makes a complete orbit and in 16 days covers the total globe. The swath is 185 km and data are

segmented in 185 km x 180 km scenes. The innovations in the monitoring unit of Landsat 8 are the Operational Land Imager (OLI) and the Thermal Infrared Sensor (TIRS), that combines historical features with new technology [13]. The OLI is made as a push-broom sensor with a four-mirror telescope, which takes data with 30 meters in the visible, near infrared, and shortwave infrared wavelength regions and with 15 meters in the panchromatic band. There are two new bands: the deep-blue band for coastal water and aerosol studies (band 1), and the Cirrus (band 9) for cirrus cloud detection. The TIRS accumulates data in two long wavelength thermal infrared bands 100-meter spatial resolution. Data will be collected simultaneously in the same area by OLI and TIR sensors [14].

Fig. 1 Artist concept of Landsat 8 (source: NASA-USGS)

The acquisition bands of Landsat 8 are reported in Table 1.

TABLE. 1. OLI Bands Designation

Spectral Bands	Description	Wavelength	Resolution
Band 1	Costal	0. 433-0. 453μm	30m
Band 2	Blue	0. 450-0. 515μm	30m
Band 3	Green	0. 525-0. 600μm	30m
Band 4	Red	0. 630-0. 680μm	30m
Band 5	NIR	0. 845-0. 885μm	30m
Band 6	SWIR-1	1. 560-1. 660μm	30m
Band 7	SWIR-2	2. 100-2. 300μm	30m
Band 8	Pan	0. 500-0. 680μm	15m
Band 9	Cirrus	1. 360-1. 390μm	30m
Band 10	TIR-1	10. 6-11. 2μm	100m
Band 11	TIR-2	11. 5-12. 5μm	100m

For this application a clip of two Landsat 8 OLI images concerning the Province of Naples (Campania Region) and acquired respectively in Red and NIR bands on Jul 29, 2013 were considered.
The clipped scene extends 70470 m x 55410 m (UTM/WGS84 plane coordinates-33T zone: E1 = 402915 m, N1 = 4541445 m, E2 = 473385 m, N2 = 4486035 m). Those data were downloaded from USGS official web site [15].
Territorial framework of the considered area is reported in Figure 2 while its RGB visualization using Landsat 8 OLI images is reported in Figure 3.

Fig. 2 Territorial framework of the considered area

TOA reflectances and NDVI calculation
Firstly Landsat data were converted from DNs to reflectance using the formula published in USGS Landsat 8 Product and show below:

$$\rho\lambda' = M_\rho Q_{cal} + A_\rho$$

where:
$\rho\lambda'$= TOA planetary reflectance, without correction for solar angle (note that $\rho\lambda'$ does not contain a correction for sun angle);
M_ρ= Band-specific multiplicative rescaling factor from the metadata (REFLECTANCE MULT BAND x, where x is the band number);
Q_{cal}= Quantized and calibrated standard product pixel values (DNs);
A_ρ= Band-specific additive rescaling factor from the metadata (REFLECTANCE ADD BAND x, where x is the band number).
Then TOA reflectance with a correction for the sun angle was calculated using the formula

$$R_\lambda = \frac{\rho\lambda'}{\sin\theta_{SE}}$$

where:
R_λ= TOA planetary reflectance;
θ_{SE}= Local sun elevation angle; the scene center sun elevation angle in degrees is provide in the metadata (SUN_ELEVATION).
Both formulas were applied using Raster calculator, the ArcGIS tool included in Spatial Analyst that permits to perform multiple tasks, mathematical calculations using operators and functions, selection queries, or development in Map Algebra syntax.
The NDVI was obtained as the normalized difference between the TOA spectral reflectances in the OLI red (R_{RED}) and infrared (R_{NIR}) bands as follows:

$$NDVI = \frac{(R_{NIR} - R_{RED})}{(R_{NIR} + R_{RED})}$$

Results and discussion

NDVI file was classified in three classes: water, soil and vegetation; thresholds were calculated using Maximum Likelihood algorithm, one of the well-known parametric classifiers used for supervised classification [16], which application with Map Algebra GIS tools is described in the case of shadow detection in [17]. Particularly several training sites for the chosen three classes and the resulting different spectral signatures were taken into account to define the thresholds in empiric way. The resulting map is visible in Figure 4.

To define the thematic accuracy of the results [18], [19], [20], several test sites were considered so to assess the performance of the classification: the values of the Producer's Accuracy, User's Accuracy and Overall Accuracy related to the resulting confusion matrix [21], [22] are reported in Table 2.

TABLE. 2. Accuracy for NDVI classification

.

Overall %	**Producer's Accuracy %**		
92. 57	**Water**	**Soil**	**Vegetation**
	100	93. 00	85. 71
	User's Accuracy %		
	Water	**Soil**	**Vegetation**
	100	92. 33	86. 87

Fig. 3 The RGB composition of the Landsat OLI images (2, 3, 4) of the considered area

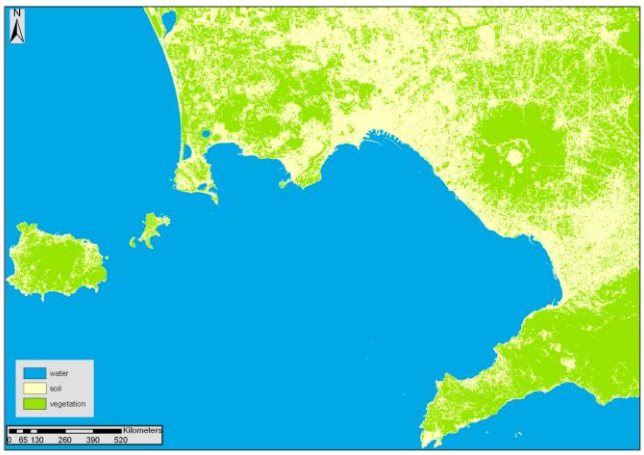

Fig. 4 NDVI classification

The classification showed high performance to identify the class of water while the accuracy of the results was lower for the other two classes; in fact the classifier in some areas caused confusion between vegetation and soil. Details of NDVI classification and the same area in RGB true color composition are reported in Figure 5, with the features of the test areas in this zone.

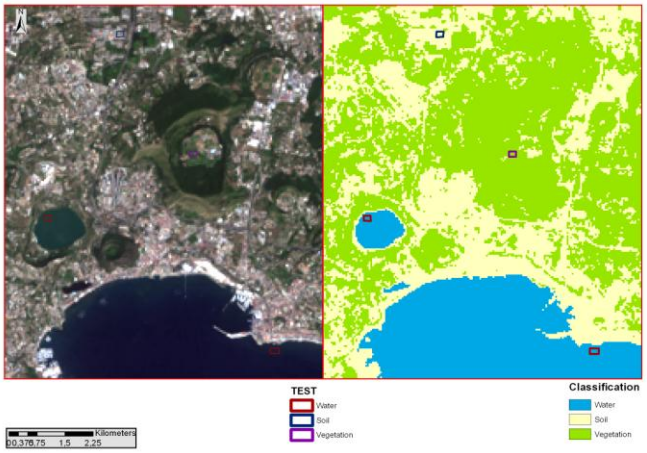

Fig. 5 A detail of: a) Areas Tests on RGB image; b) the NDVI classification of the same zone

Conclusion

This study shows the advantage of GIS to process satellite images and calculate TOA as well as NDVI. GIS tools can be used in a simple way and to speed up repetitive tasks. Particularly raster calculator permits both to operate with a single raster as well as with two (or more) images: in the first case it is possible to transform each original DNs matrix into reflectance (TOA); in the second case NDVI can be easily implemented. In this paper Landsat 8 OLI images are considered, but the same procedure can be extended to other satellite images.

References

[1] C., Barroso, and I., Monteiro, "Monitoring vegetation from space. EUMeTrain Project", Available: http://www. eumetrain. org/data/3/36/print. htm, 2010.

[2] C. J., Tucker, "Red and Photographic Infrared Linear Combinations for Monitoring Vegetation", Remote Sensing of Environment, Vol. 8 (2), pp. 127-150, 1979.

[3] T., Lillesand, R. W., Kiefer, and J., Chipman, "Remote sensing and image interpretation", John Wiley & Sons, 2014.

[4] B. L., Markham, and J. L., Barker, "Spectral characterization of the Landsat-4 MSS Sensors", Photogrammetric Engineering and Remote Sensing, 49(6), pp. 811−833, 1983.

[5] J. W., Rouse, R. H., Haas, J. A., Schell, and D. W., Deering, "Monitoring vegetation systems in the Great Plains with ERTS", Third ERTS Symposium, NASA SP-351 I, pp. 309-317, 1973.

[6] W. B., Cohen, and S. N., Goward, "Landsat's role in ecological applications of remote sensing", Bioscience, Vol. 54 (6), pp. 535−545, 2004.

[7] Y., Ke, J., Im, J., Lee, H., Gong, and Y., Ryu, "Characteristics of Landsat 8 OLI-derived NDVI by comparison with multiple satellite sensors and in-situ observations", Remote Sensing of Environment, Vol. 164(2015), pp. 298-313, 2015.

[8] G., Firl, and J. L., Carter, "Lesson 10: Calculating Vegetation Indices from Landsat 5 TM and Landsat 7 ETM+ Data", Colorado State University, Available: http://ibis. colostate. edu/WebContent/WS/ColoradoView/TutorialsDownloads/CO_RS_Tutorial10. pdf.

[9] C., Parente, "TOA reflectance and NDVI calculation for Landsat 7 ETM+ images of Sicily", In Proceedings in EIIC-The 2nd Electronic International Interdisciplinary Conference (No. 1), 2013.

[10] ArcGIS, E. S. R. I. "10. 1" Redlands, California: ESRI, 2012.

[11] U. S. Geological Survey, "Landsat 8 (L8) Data Users Handbook", (June 2015), Version 1. 0, pp. 61-62, 2015.

[12] R. A., Byrnes, "Landsat-A Global Land-Imaging Program",: U. S. Geological Survey Fact Sheet No. 2012-3057, 2012.

[13] U. S. Geological Survey, "Landsat Continuing to Improve Everyday Life", NASA, 2013, available: http://landsat. gsfc. nasa. gov.

[14] J. R., Irons, J. L., Dwyer, and J. A., Barsi, "The next Landsat satellite: The Landsat data continuity mission", Remote Sensing of Environment, 122(2012), pp. 11-21, 2012.

[15] U. S. Geological Survey, "Earthexplorer", Available: http://earthexplorer. usgs. gov., 2015.

[16] J. R., Otukei, and T., Blaschke, "Land cover change assessment using decision trees, support vector machines and maximum likelihood classification algorithms", International Journal of Applied Earth Observation and Geoinformation 12 (2010): S27-S31, 2010.

[17] C., Meneghini, and C., Parente, "Application for shadow removal from Geo Eye-1 RGB composition", International Journal of Applied Engineering Research, ISSN 0973-4562 Volume 10, Number 6 (2015), pp. 15833-15842, 2015.

[18] J. B., Campbell, "Introduction to remote sensing", (2nd ed.), London: Taylor and Francis, 2002.

[19] G. M., Foody, "Status of land cover classification accuracy assessment", Remote sensing of environment, 80(1), pp. 185-201, 2002.

[20] R. G., Congalton, and K., Green, "Assessing the accuracy of Remotely Sensed Data-Principles and Practices", CRC Press-Tailor & Francis Group, FL (USA), II edition, 2009. ISBN: 978-1-4200-5512-2, 2009.

[21] S. V., Stehman, "Selecting and interpreting measures of thematic classification accuracy", Remote sensing of Environment, 62. 1 (1997): 77-89, 1997.

[22] P., Maglione, C., Parente, R., Santamaria, and A., Vallario, "Modelli tematici 3D della copertura del suolo a partire da DTM e immagini telerilevate ad alta risoluzione WorldView-2", Rendiconti online della Società Geologica Italiana, Volume 30, pp. 33-40, ISSN 2035-8008, 2014.